



Effect of secondary organic aerosol coating thickness on the real-time detection and characterization of biomass burning soot by two particle mass spectrometers

Adam T. Ahern,¹ R. Subramanian,¹ Georges Saliba,¹ Eric M. Lipsky,^{1,2} Neil M. Donahue,¹ Ryan C. Sullivan^{1,*}

5 ¹Center for Atmospheric Particle Studies, Carnegie Mellon University, Pittsburgh, PA, USA, 15213

²Penn State Greater Allegheny, 4000 University Drive, McKeesport, Pennsylvania 15132, USA

*Corresponding Author: R.C. Sullivan (rsullivan@cmu.edu)

10 Biomass burning is a large source of light-absorbing refractory black carbon (rBC) particles with a wide range of morphologies and sizes. The net radiative forcing from these particles is strongly dependent on the amount and composition of non-light absorbing material internally mixed with the rBC, and on the morphology of the mixed particles. Understanding how the mixing state and morphology of biomass-burning aerosol evolves in the atmosphere is critical
15 for constraining the influence of these particles on radiative forcing and climate. We investigated the response of two commercial laser-based particle mass spectrometers, the VUV ablation LAAPTOF and the IR vaporization SP-AMS, to monodisperse biomass-burning particles as we sequentially coated the particles with secondary organic aerosol (SOA) from α -pinene ozonolysis. We studied three mobility-selected soot core sizes, each with a number of
20 successively thicker coatings of SOA applied. Using IR laser vaporization, the SP-AMS had different changes in sensitivity to rBC compared to potassium as a function of applied SOA coatings. We show that this is due to different effective beam widths for the IR laser vaporization region of potassium versus black carbon. The SP-AMS's sensitivity to BC mass was not observed to plateau following successive SOA coatings, despite achieving high OA:BC mass
25 ratios > 9. We also measured the ion fragmentation pattern of biomass-burning rBC and found it changed only slightly with increasing SOA mass. The LAAPTOF demonstrated a linear average organic matter ion signal in response to the condensed SOA mass on individual particles, despite the inhomogeneity of the particle core compositions. This demonstrates that the LAAPTOF can obtain quantitative mass measurements of aged soot particle composition
30 from realistic biomass-burning particles with complex morphologies and composition.



1 Introduction

Particles containing black carbon (BC) are largely anthropogenic and have the third largest warming effect on the planet, after CO₂ and methane (Bond et al., 2013; Ramanathan and Carmichael, 2008). This makes BC-containing particles a likely target for climate change mitigation policy (Anenberg et al., 2012). However, there is high uncertainty regarding the climate forcing of BC, and thus any potential benefits from BC control technologies and policies (Jacobson, 2001). The uncertainty stems from the variable optical, chemical, and physical properties of BC, which affect particle radiative properties and lifetime, respectively. The properties of BC-containing particles can change as atmospheric oxidants react with gas-phase vapors; the products of these reactions can condense onto the light-absorbing aerosol. Although this condensed material may not absorb light itself, it can affect the lifetime and cloud-nucleation ability of the BC-containing particle, and increase the internally mixed BC absorption of sunlight by as much as a factor of two (Bond et al., 2013; Chung and Seinfeld, 2002; Jacobson, 2001; Lack et al., 2009; Moffet et al., 2008; Ramanathan and Carmichael, 2008).

The burning of non-fossil-fuel biomass, either as biofuel, agricultural refuse, or in wildfires, is the largest source of light-absorbing BC-containing particles globally. However, the effect of aging on the biomass burning aerosol (BBA) is not well characterized (Bond et al., 2013). In some cases, co-emitted organic gases become oxidized and condense on the BBA, simultaneously reducing BBA atmospheric lifetime and increasing BBA light absorptivity (Lack et al., 2009; Mikhailov et al., 2006; Yokelson et al., 2009). In other smoke plumes, there has been no observed increase in organic matter (OM) with aging, and in a few cases a decrease in OM has been reported, likely due to dilution-induced evaporation (Cubison et al., 2011; May et al., 2013). In order to identify the contribution of various chemical processes to the compositional changes in BC-containing particles, measurements of particle composition must be carried out with a temporal resolution similar to or faster than the timescale of the chemical processes. Improved mass measurements of BC and internally mixed material will enable more accurate model simulations that constrain the climate forcing by black carbon and other aerosol components.

Particle mass spectrometers provide information about the chemical composition of atmospheric aerosols with a time resolution comparable to their transformation processes. In this paper we investigate the response of two commercial laser-based particle mass spectrometers to the systematic condensation of secondary organic aerosol (SOA) onto complex biomass-burning soot particles. One instrument is an infrared laser vaporization soot-particle aerosol mass spectrometer (SP-AMS, Aerodyne Research Inc.), while the other is a laser desorption ionization single-particle mass spectrometer (LDI-SP-MS) known as the laser ablation aerosol particle time of flight mass spectrometer (LAAPTOF, Aeromegt GmbH). Both instruments provide chemical information regarding the core composition of BBA particles as well as secondary condensed components on a time scale of ten minutes or less. However, each has quantitative challenges related to particle mixing state and morphology that are the subject of ongoing research (Corbin et al., 2014; Onasch et al., 2015; Spencer and Prather, 2006; Willis et al., 2014). Herein we evaluate the ability of the two instruments to measure the composition of BBA composed of both a rBC core and SOA coating, as we simulate atmospheric aging by coating primary BBA particles with complex secondary organic material in a chamber reactor.



We confirm that significant SOA coatings on rBC cause only small changes in the ion fragmentation patterns of elemental carbon in the SP-AMS. We show that the infrared laser beam waist in the SP-AMS has a different effective beam width and therefore different detection efficiency for alkali metals versus rBC. The feasibility of quantitative measurements of organic matter (OM) by the LAAPTOF in complex and realistic particles containing BBA, rBC, and SOA was also investigated. We demonstrate that the LAAPTOF measures a linear increase in OM ion signal in response to the SOA mass condensed on BBA particles. This is significant given the especially complex composition of BBA, and is highly encouraging for achieving mass quantitative single-particle measurements of other complex ambient particle matrices.

1.1 Characterization of carbonaceous aerosol by particle mass spectrometry

The SP-AMS is a variant of the conventional aerosol mass spectrometer that includes an intracavity infrared (IR) laser that can vaporize light-absorbing refractory material. Refractory is an operationally defined term describing any material not vaporized by the 600 °C heater in a conventional AMS. With the IR laser the SP-AMS can measure two key refractory species that are used as inert, non-volatile tracers for biomass burning: refractory black carbon (rBC), and potassium (Andreae, 1983; Hennigan et al., 2011; Lee et al., 2016). The sensitivity of the SP-AMS to rBC has been shown to increase with the addition of organic coatings to BC-containing particles. Willis et al. (2014) showed that the increased sensitivity was due to increased overlap between the particle beam and the IR beam that vaporizes the particles. The particles become more tightly focused by the aerodynamic lens inlet with increasing coating thickness and thus sphericity, causing a larger portion of the particle beam to intersect with the IR laser beam. The fraction of BC-containing particles that are vaporized by the IR laser is defined by Onasch et al. (2012) as the shape-dependent collection efficiency, E_s , and is the determining factor for the sensitivity of the SP-AMS to rBC. Willis et al. (2014) measured the E_s for rBC using a beam-width probe with a BC aerosol calibration standard (Regal Black, Cabot) coated to varying degrees with dioctyl sebacate (DOS), a surrogate for primary or hydrocarbon-like OM. They observed that the E_s was less than unity for uncoated, collapsed rBC particles such as Regal Black, but that for urban ambient particles and DOS-coated Regal Black, E_s was close to one. However, real-world BBA has a different composition than Regal Black, with particles that are less spherical and that contain inorganic salts (e.g. potassium chloride) that may be internally or externally mixed with rBC (Huffman et al., 2005; Li et al., 2003; Onasch et al., 2012). We will show that as BBA is coated with OM, the SP-AMS ion signal response to the mass of potassium and BC increases. Furthermore, we will show that the SP-AMS response to potassium increases more rapidly than that for rBC for equivalent amounts of OM coating, despite the species being internally mixed.

Most chemical components in the SP-AMS undergo sequential vaporization followed by 70 eV electron ionization of only the vapors. This allows for extensive but reproducible molecular fragmentation and subsequent classification and detection of the resulting ions in the high-resolution time-of-flight mass spectrometer. The IR laser vaporization enables the subsequent ionization and thus detection of refractory material in particles containing BC that strongly absorbs the IR laser energy. The vapors produced by the IR laser are ionized by the same electron source used in the normal operation where vaporization is performed only with the 600 °C heater. The reproducibility of the ion fragmentation by electron ionization has led researchers to investigate the possibility of using the ratios of the various detected elemental



carbon (EC) fragments (C_x^+) to perform source apportionment of rBC. Corbin et al. (2014) showed that fullerene-rich particles produced a higher ratio of C_4^+ -to- C_3^+ than did particles from higher temperature combustion, which did not contain substantial fullerenes. Onasch et al. (2015) confirmed that fragmentation of larger graphitic molecules was a minor source of C_4^+ cations in addition to the direct ionization of vaporized rBC. This suggests that the elemental carbon (EC) fragmentation pattern could be used to differentiate between rBC generated from different types of combustion (e.g. diesel vs. biomass combustion). Here we investigate the effect of atmospheric aging in the form of OM coatings on these EC ion ratios.

The LAAPTOF is a laser desorption/ionization single-particle mass spectrometer (LDI-SP-MS) using a VUV excimer laser pulse to ablate and ionize individual particles simultaneously. This enables the analysis of a wider range of particle compositions and types than is possible with the AMS, even when the IR laser is used. High time resolution measurements of individual particles are achieved; an aerodynamic size and bipolar mass spectrum can be obtained for each particle. LDI-SP-MS also provides much greater mass sensitivity compared to the less efficient electron ionization scheme because the laser ionization produces many more ions than electron ionization per mole of analyte (Farmer and Jimenez, 2010; Murphy, 2007; Pratt and Prather, 2012; Sullivan and Prather, 2005). However, the large number of ions produced per particle can result in poor MS resolution and/or ion plume chemistry after desorption/ionization. The molecular fragmentation is also less reproducible compared to 70 eV electron ionization due to laser shot-to-shot variability, inhomogeneity of the laser pulse, and varying optical properties of individual particles. Generation of ions directly from each particle introduces important matrix effects where the particle's composition and properties strongly dictate its interaction with the VUV laser pulse, the distribution of laser energy to the particle's constituents, and the resulting ion signal and fragmentation (Gross et al., 2000; Mansoori et al., 1996; Reinard and Johnston, 2008; Steele et al., 2005; Thomson et al., 1997; Wenzel and Prather, 2004).

Despite these challenges, LDI-SP-MS can obtain quantitative measurements of individual particle composition and its evolution. Effective demonstrations of data analysis strategies for achieving quantitative LDI-SP-MS measurements include restricting the analysis to particles of a similar particle type based on their mass spectrum, normalization of ion peak areas to total ion signal, the use of ion peak area ratios, sensitivity calibration by comparison to co-located speciated mass measurements, and signal averaging over numerous individual measurements (Bhave et al., 2002; Fergenson et al., 2001; Gross et al., 2000; Healy et al., 2013; Jeong et al., 2011; Pratt and Prather, 2012; Spencer and Prather, 2006; Sullivan and Prather, 2005; Sullivan et al., 2009). Although the ion plume chemistry can complicate analysis, the species known to cause ion-plume effects (e.g. water, inorganic salts) are generally present in the mass spectra and can thereby inform the analysis (Murphy, 2007; Murray and Russell, 1994; Neubauer et al., 1998). In this study, we account for laser shot-to-shot inconsistencies by averaging over particles of similar size and composition.

Spencer and Prather (2006) used graphite spark-generated soot with condensed unleaded fuel to calibrate the ATOFMS LDI-SP-MS and found a linear relationship between the ratio of summed select OM cation signals to summed select elemental carbon (EC) cation signals, as the mass of OM condensed on the EC was increased. Before such analysis can be used with confidence on realistic combustion BBA and complex SOA, two key differences



between soot and BBA must be addressed, namely the variable morphology of BBA and the presence of inorganic salts. Inorganic salts, such as the potassium chloride observed in BBA, are very readily ionized (Li et al., 2003; Reid et al., 2005; Zauscher et al., 2013). They therefore can generate a dense ion cloud that may reduce MS resolution and can interfere with the formation/detection of other ions (Murphy, 2007). The presence of potassium, the irregular shape, and strongly light-absorbing nature of BBA presents an especially complex matrix for LDI-SP-MS. We evaluated the ability of the LAAPTOF with its 193 nm laser to generate and detect OM ion signal proportional to the mass of realistic SOA condensed on a BBA particle.

2 Experimental Methods

2.1 Experimental particle generation and conditioning

In Figure 1 we display the experimental setup for the generation, coating, and characterization of monodisperse biomass-burning aerosol particles. The combustion of solid biomass fuel generates particles with shapes and compositions that vary more widely than those produced from controlled, well-mixed internal-combustion engines (Reid et al., 2005; Schwarz et al., 2008). Relative to engine exhaust soot, biomass-burning particles may have higher surface area (due to the fractal-like shape of soot particles) and more non-carbonaceous components, such as inorganic salts (Li et al., 2003; Reid and Hobbs, 1998). For these experiments, we burned European white birch bark in a cookstove and sampled the smoke from the flaming phase 1 m above the fire through 1/2" o.d. stainless-steel tubing. We removed the gas-phase organics from the smoke by pulling polydisperse smoke through a 20 °C annular activated-carbon denuder with a diaphragm pump. The same pump then pushed the denuded aerosol sample through a series of ⁸⁵Kr neutralizers and a differential mobility analyzer (DMA; TSI, model 3081) with a sample flow of 4.0 Lpm and a non-circulating sheath flow of 18 Lpm to select a narrow range of electrical mobility particle diameters. We then injected the

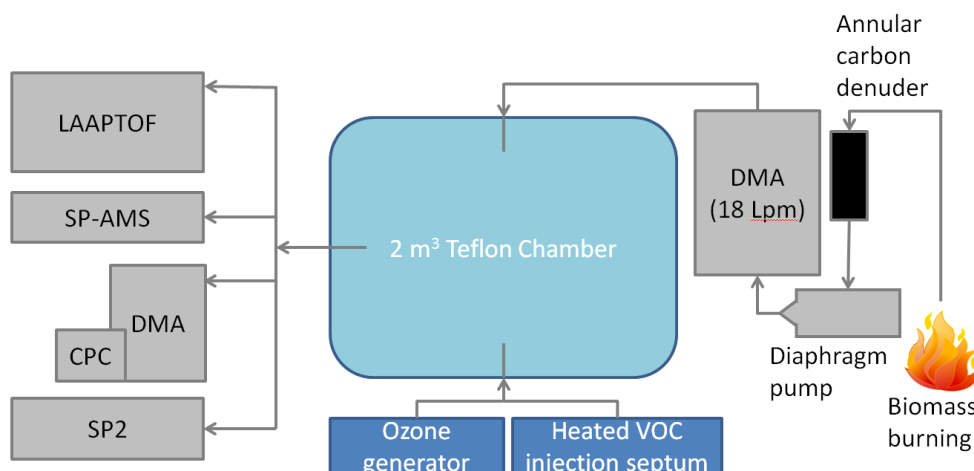


Figure 1. Experimental setup including size-selected biomass-burning aerosol generation, environmental aging chamber for sequential coating with α -pinene SOA, and subsequent online characterization with particle instrumentation.



monodisperse soot particles into a 2 m³ Teflon chamber at a rate of 4.0 Lpm until the concentration was between 2,000 and 14,000 particles cm⁻³. This typically took less than 30 minutes. During this time, we continuously fueled the fire to maintain flaming conditions. Before soot injection, we partially filled the chamber with clean filtered dry air. Although the diaphragm pump generated some small particles (with mobility diameters less than 50 nm), they were smaller than the selected soot particles (143 nm to 220 nm mobility diameter) and thus not transmitted through the DMA into the chamber.

We characterized the nascent soot particles with a suite of particle instruments described below and confirmed that the particles were nearly monodisperse; doubly-charged particles were always less than 10% by number. We then injected precursor gases for SOA formation. We generated ozone by flowing oxygen through a corona-discharge ozone generator (Azco, HTU500AC) until the chamber concentration reached ~300 ppb. We measured the ozone concentration with a UV photometric ozone monitor (Dasibi, 1008-PC). We injected 0.1 or 0.2 µL aliquots of α-pinene (Sigma Aldrich, >99%) through an air-tight heated septum flushed with clean air. We used serial injections of α-pinene to generate successively thicker SOA coatings on the soot cores. Chamber experiments with several steps of SOA production typically lasted 3-4 hours, stopping after homogenous nucleation prevented additional coating of soot seeds.

2.2 Particle component mass measurements

We characterized the soot and the SOA coatings using a number of different methods. We used three instruments to measure the refractory black carbon (rBC): a Droplet Measurement Technologies Single Particle Soot Photometer (SP2) (Schwarz et al., 2010; Stephens et al., 2003); a laser desorption/ionization single-particle mass spectrometer (LDI-SP-MS) – the Laser Ablation Aerosol Particle Time-Of-Flight (LAAPTOF) mass spectrometer; and an Aerodyne Soot-Particle High Resolution Aerosol Mass Spectrometer (SP-AMS) (Onasch et al., 2012). Extensive descriptions of the SP2 and SP-AMS instruments are available elsewhere and thus we provide only a brief overview. For the LAAPTOF we describe the salient features below; a more detailed discussion of the LDI-SP-MS technique is available in the form of a review article by Murphy (2007), and literature descriptions of other closely related instruments (Marsden et al., 2016; Pratt et al., 2009; Sullivan and Prather, 2005; Thomson et al., 2000; Zelenyuk et al., 2009).

The LAAPTOF is a commercially available single-particle mass spectrometer (Aeromegt, GmbH) that uses laser desorption/ionization to generate positive and negative ions from individual particles that are subsequently detected by a bipolar time-of-flight mass spectrometer (TOFWerk, AG) (Gemayel et al., 2016; Marsden et al., 2016). The particles are focused into the ionization region by an aerodynamic lens. Normally the particle time-of-flight is measured by light scattering between two 405 nm continuous-wave lasers (OBIS, Coherent Inc.) to determine the velocity of each particle and thus its vacuum aerodynamic diameter. The particle is then ablated and ionized with an eight nanosecond pulse from a VUV 193 nm excimer laser (EX5, GAM Laser, Inc.) that is triggered immediately by the second particle light scattering event. The VUV pulse travels coaxially up the particle beam and hits the particle in the ion extraction region, coincident with and orthogonal to the second light scattering laser beam. During these experiments, the 405 nm scattering lasers were not operational, and instead we free-fired the excimer laser at 10 Hz with an average laser pulse energy of 2.0 mJ. We set and



periodically confirmed the VUV laser power using a laser power meter (EnergyMax, Coherent, Inc.).

5 Single-particle analysis provides valuable insight into the physical and chemical evolution of biomass-burning plumes as they are diluted by entrainment of background air, and undergo transformation processes during transport. Single-particle analysis also facilitates the determination of contributions from biomass-burning particles to aerosol loading for source apportionment, and can reveal changes in the mixing state of biomass-burning particles as they age (Chen et al., 2014; Moffet et al., 2008; Silva et al., 1999; Zauscher et al., 2013). Although laser desorption/ionization (LDI), such as that used by the LAAPTOF, is often regarded as a semi-quantitative method, there are numerous examples demonstrating that it can be mass quantitative for constrained systems where similar particle matrices are studied (Mansoori et al., 1994; Spencer and Prather, 2006; Sullivan et al., 2007, 2009). Quantitative mass measurements using (LDI-SP-MS) are difficult because of the particle matrix effects that influence how much energy is absorbed by a given particle and subsequently the production and fate of the generated ions (Murphy, 2007; Steele et al., 2005; Sullivan and Prather, 2005). Calibration of the LDI-SP-MS ion-signal response to particles of known composition is also required to yield mass-quantitative component measurements. The SOA-coated soot experiments we present here provide a unique opportunity to characterize the response of the LAAPTOF to realistic biomass-burning cores coated with complex and realistic biogenic SOA, where the masses of rBC and OM are well constrained.

20 The SP2 rapidly heats individual rBC-containing particles as they pass through an intracavity IR laser beam, and then measures the intensity of emitted thermal radiation resulting from particle incandescence. The rBC mass of each particle is proportional to this light intensity. We calibrated the SP2 rBC mass response with fullerene soot that we size-selected using a DMA. We previously measured the batch-specific effective density of this soot sample using a Cambustion Centrifugal Particle Mass Analyzer (Gysel et al., 2011; Slowik et al., 2007). We measured the particle concentration during these calibrations using a Condensation Particle Counter (TSI model 3772). Further details are provided by Saliba et al. (2016), where the optical properties of the coated rBC particles produced in these experiments are presented.

30 Particles are focused into a collimated beam for transmission into the SP-AMS using an aerodynamic lens very similar to the LAAPTOF. The SP-AMS uses the same IR laser as the SP2 to vaporize rBC along with any internally mixed components; the vapors are then ionized by 70 eV electrons from a tungsten filament and the ions analyzed by time-of-flight mass spectrometry. The SP-AMS also contains a tungsten heater kept at 600 °C for particle thermal desorption, identical to the conventional AMS design. Unless stated otherwise, we operated the SP-AMS with both the IR laser and the conventional heater on for all experiments described here. The largest uncertainty in mass measurements of rBC by the SP-AMS is the particle collection efficiency, which is determined by the particle shape and size. Particle beam divergence (E_s) has been shown to be the largest uncertainty for SP-AMS mass measurements using the IR laser. It is caused by the incomplete overlap of the particle beam and the IR laser beam (Huffman et al., 2005; Onasch et al., 2012; Willis et al., 2014). A perfectly collimated particle beam would result in all of the rBC-containing particles passing through the center of the Gaussian IR laser beam energy profile, where it is most intense. However, the particle beam can spread because small and/or irregularly shaped particles diverge from an ideal beam

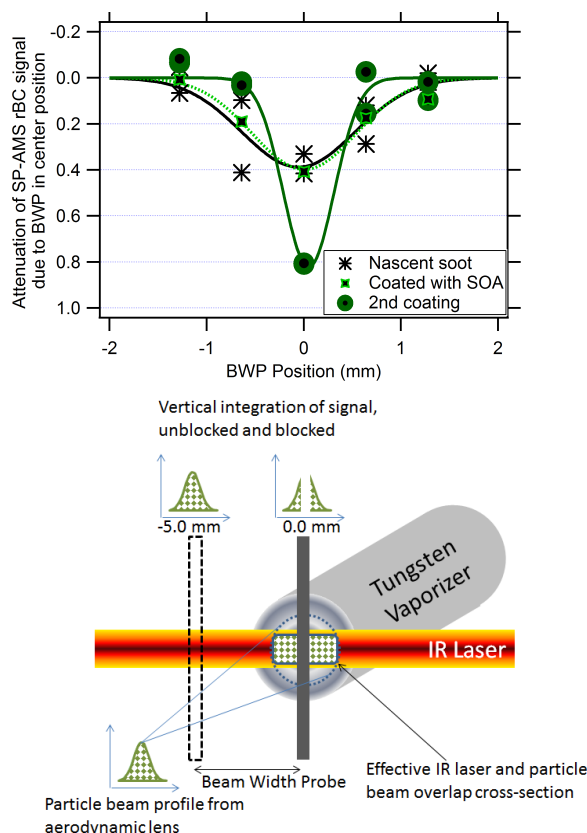


Figure 2. The particle beam-width probe blocks a fraction of the particles that would have been vaporized by the IR laser and thus the probe attenuates the elemental carbon ion signal (C_x^+) for rBC containing particles. We used six probe positions to establish the particle-beam width. The measured ion signal is the integrated Gaussian profile shown at the top of the schematic. The difference between the unblocked ($x = -5.0$ mm) and blocked (0.0 mm) green integrated Gaussian profile plots is the attenuation for that beam width probe blocking-position, plotted as the y-axis on the top figure. The top panel shows the attenuation of nascent uncoated soot (black asterisks), soot with a single coating of SOA (black and light green crosses), and soot with a second coating of SOA (black and dark green circles). A wider Gaussian particle beam shape determined by the beam-width probe analysis indicates the aerosol has a small diameter and/or a larger (less spherical) particle shape factor, and therefore $E_s < 1$.

profile. This divergence is due to Brownian diffusion or uneven drag distribution on the particles as they leave the aerodynamic lens (Huffman et al., 2005; Liu et al., 1995). The collection efficiency for non-refractory material not mixed with IR-laser absorbing rBC (components that promptly evaporate at 600 °C) is determined by the particle bounce off of the heater. Note that the cross-sectional area of the heater is much larger than that of the IR laser beam. Therefore, particle detection of refractory components such as rBC in the SP-AMS by IR vaporization is more sensitive to particle shape than is the detection of non-refractory components vaporized by the 600 °C heater.

We determined the fraction of total particle mass undetected by the SP-AMS due to diverging, light-absorbing particles missing the IR laser beam. We did this by measuring the ion



signal from refractory species (elemental carbon or potassium) while sequentially blocking portions of the particle beam with a thin piece of wire ($\varnothing = 0.41$ mm), called the beam-width probe. We compared the signal with the beam-width probe in place to the signal observed when the wire was not obstructing any of the particle beam (Huffman et al., 2005; Willis et al., 2014). We show this schematically in Figure 2 for the carbon cation signal, C_x^+ (where x is a positive integer). The ratio of the partially blocked signal to the unblocked signal, hereafter referred to as the attenuation with the beam-width probe, indicates how narrow the particle beam is. If the measured attenuation is high, then in the absence of the beam-width probe, most of the particles will pass through the most intense IR laser region and be vaporized. If the attenuation is low, then some of the particles will miss the laser and the refractory material will not be detected. As the beam-width probe is wider than the effective width of the IR laser for rBC (a Gaussian distribution with $\sigma = 0.18$ mm), anything less than complete attenuation of the measured ion signal when the beam-width probe is at the center position indicates that some of the EC mass on particles containing rBC will not be detected. Therefore, E_s will be < 1 (Willis et al., 2014). However, as we will show, vaporization of potassium occurs with a larger effective IR beam width, and thus E_s is larger for potassium than rBC.

2.3 Particle mobility measurements and calculations

We classified the size distribution of the biomass-burning aerosol (BBA) with a Scanning Mobility Particle Sizer (SMPS; TSI Inc., model 3081 DMA and 3772 CPC) that measures particle mobility diameter (d_{mob}) size distributions, and with the SP-AMS that measures particle vacuum aerodynamic diameter (d_{va}) in addition to composition. The SP-AMS measures the vacuum aerodynamic diameter by accelerating particles into a vacuum and measuring the time to ion detection after a particle passes through a rotating 1% slit chopper. We calibrated the particle time of flight measurements using polystyrene latex spheres vaporized using the conventional tungsten heater in the SP-AMS (Jayne et al., 2000). It is important to note that for the fractal-like nascent soot particles, the terms d_{mob} and d_{va} do not fully describe the physical shape of a particle. Rather, they describe the relationship between the drag force on that particle compared to either a counterbalancing electrostatic force for d_{mob} or the acceleration modulated by the particle mass for d_{va} (DeCarlo et al., 2004).

In Figure 3 we show aerodynamic size distributions for particles originally selected with a DMA at 143 nm d_{mob} . Though the nascent particles were monodisperse in mobility space, the d_{va} distribution for the nascent soot particles was much wider than the d_{mob} distribution. This is probably due to the range of particle masses and shapes that can exist at a given d_{mob} for highly irregular nascent soot. The d_{va} size range narrowed following the addition of SOA coatings, likely reflecting the increasing uniformity as the irregularly shaped particles became coated with SOA. When measuring the mobility size distribution, we adjusted the sheath flow of the SMPS to ensure that we captured the complete aerosol size distribution, at times operating at sheath-to-sample flow ratios as low as 5:1. Although the lower sheath-to-sample flow ratio reduces the SMPS size resolution, it does not affect the accuracy of the mode size determination.

As a nascent soot particle becomes coated with SOA, the particle grows and gains organic mass. Thus d_{mob} , d_{va} , and the organic mass per particle all increase. We calculated the SOA mass per particle (m_{SOA}) from mobility and mass measurements following the method described in Slowik et al. (2004), with some differences as described here. In addition to d_{mob} and d_{va} , we measured the single-particle black carbon mass (m_{rBC}) with the SP2. The SP2 also

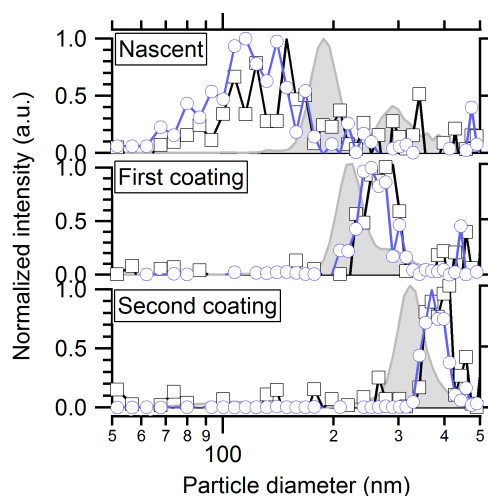


Figure 3. Normalized particle size distributions for coating experiments from two instruments. Traces are mass distributions vs. vacuum aerodynamic diameter (d_{va}) for two refractory species measured by the SP-AMS, potassium (purple circles) and rBC (black squares). The filled-in gray curve is the volume distribution (d^3) versus mobility diameter (d_{mob}) measured by the SMPS. Measurements of the original uncoated nascent biomass-burning soot particles are shown in the top panel, while the middle and bottom panel show measurements after we applied the first and second SOA coatings, respectively. The uncoated particles had broad mass distributions with modes well below the mobility volume mode indicating fractal particles with a wide variability in particle shape. The mass distribution narrowed and overtook the volume distribution following condensation of SOA because the particles became more spherical and homogeneous with respect to shape and composition, with a density greater than 1.0 g/cm^3 .

confirmed that $> 97\%$ of the nascent particles were composed of significant amounts of black carbon. We assumed that the black-carbon density (ρ_{rBC}) was 1.8 g/cm^3 (Park et al., 2004). For thickly coated particles, with $m_{SOA} \gg m_{rBC}$, we assumed that the particles were effectively spherical and determined the density of the SOA (ρ_{SOA}) to be 1.3 g/cm^3 by taking the ratio of d_{mob} and d_{va} . Knowing the two densities, we then iteratively solved for the particle dynamic shape factor (χ), volume equivalent diameter (d_{ve}), and the average mass of SOA per particle (m_{SOA}) using Eqs. (1), (2), and (3) below, taking into account the Cunningham slip correction factor (C_c).

$$d_{mob} = \frac{d_{ve} C_c(d_{mob}) \chi}{C_c(d_{ve})} \quad (1)$$

$$d_{va} = \frac{d_{ve}}{\chi(\rho_0)} \left(\frac{m_{rBC} + m_{SOA}}{\frac{m_{rBC}}{\rho_{rBC}} + \frac{m_{SOA}}{\rho_{SOA}}} \right) \quad (2)$$

$$\frac{m_{rBC}}{\rho_{rBC}} + \frac{m_{SOA}}{\rho_{SOA}} = \frac{\pi}{6} * d_{ve}^3 \quad (3)$$

We neglected the contribution of ammonium, sulfate, and nitrate to particle mass and volume as they are small ($< 10\%$) relative to rBC and SOA. Unless specified otherwise, SOA mass per particle is calculated in this manner.

2.4 Effect of SOA condensation on soot particle shape

Figure 4 shows the calculated dynamic shape factor, χ , for particles as they were coated with SOA. Nascent soot particles are very fractal-like, with $\chi > 1.6$. This is within the range of previously observed soot from fuel-rich combustion (Slowik et al., 2004). For context, Schwarz

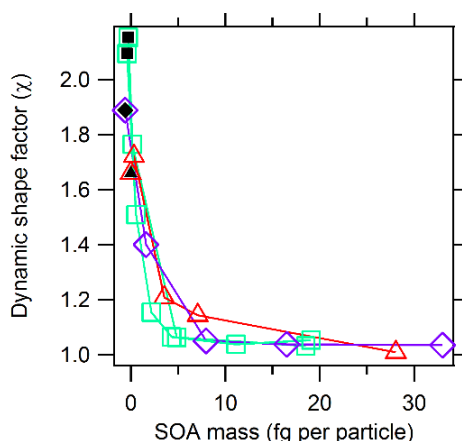


Figure 4. Dynamic shape factor (χ) of soot particles became more spherical ($\chi \rightarrow 1$) with increasing SOA mass. Nascent particles (black) were coated sequentially, and after 5 fg of SOA per particle had condensed the particles are mostly spherical in shape. Additional coatings served to increase the diameter of the now effectively spherical particles. Different colored/shaped symbols indicate different initial selected soot core mobility diameters: red triangles were initially 142 nm, teal squares were 188 nm, and purple diamonds were 220 nm.

et al. (2008) measured the thickness of coatings on ambient BBA using an SP2. The instrument was onboard an aircraft that transected a biomass-burning plume. They determined aged ambient particles with a BC core mass equivalent diameter of 200 nm had a coating thickness of 79 nm ~1 hour after emission from the biomass burning source. For comparison, we assume the BBA particles discussed in Schwarz et al. (2008) are coated with SOA with a density of 1.3 g/cm³. The SOA coating mass would then be 25.7 fg of OA mass per particle, and would result in a mostly spherical particle. Although we cannot say the particle coating observed by Schwarz et al. (2008) consisted entirely of OA mass, the volume equivalent of any secondary component such as sulfate would also result in a spherical particle shape. As shown before, because the particle shape and size influences the particle beam profile and the beam width at the IR laser, the shape factor influences the total rBC signal detected by the SP-AMS.

3 Results and Discussion

In Figure 5 we display a time series from a particle coating experiment for initially monodisperse (by mobility) particles with $d_{mob} = 143$ nm. All of the experiments followed this general pattern. We show the particle mobility size distribution from the SMPS, the rBC mass from the SP2, and the SP-AMS signal for both rBC and organic material (OM). Prior to coating ($t < 0$), the SP2 and SP-AMS rBC signals decreased as particles were lost to the chamber walls. After each α -pinene vapor injection, which drove SOA coating, the particle mobility diameter increased and there was also an increase in the SP-AMS OM signal. After the second injection ($t = 0.6$ hours), the SP-AMS rBC signal increased while the SP2-measured rBC mass concentration continued to decay, as expected due to particle wall loss. This difference demonstrates that the increase in SP-AMS rBC signal with thicker SOA coatings was almost certainly due to an



increase in the IR laser beam particle collection efficiency (E_s) of the SP-AMS, and not an increase in the actual rBC mass present in the chamber.

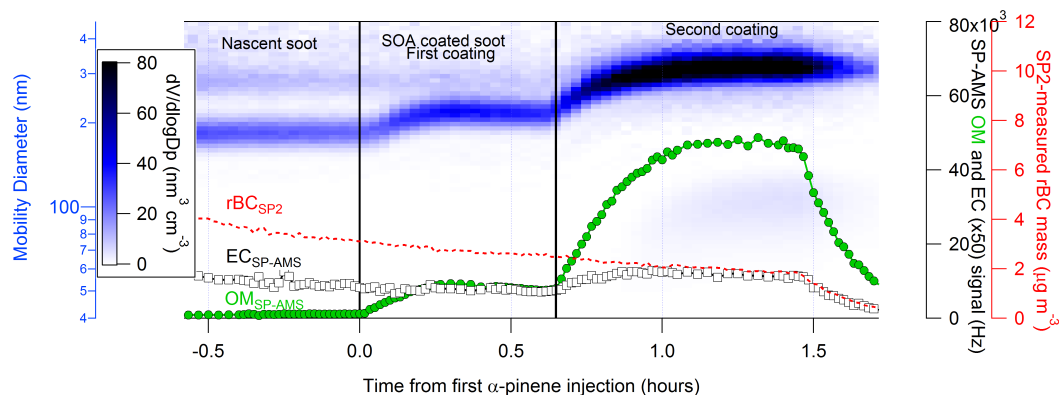


Figure 5. Monodisperse biomass soot particles to which two successive additions of SOA were applied. Fractal-like, monodisperse soot particles with initial mobility diameter of 143 nm grew via condensation of successive SOA coatings following discrete injections of α -pinene vapor (indicated by vertical lines) into a chamber containing ozone. Particle growth is evident in the volume-weighted SMPS mobility size distribution (blue-black, top) and the SP-AMS measured OM (green closed circles) and EC (black open squares) ion signal as a function of time. SP2 rBC mass measurements (red dotted line) reveal the steady decay of soot-particle mass concentration due to chamber wall loss, followed by greater loss when we purged the chamber at $t > 1.5$ hours.

3.1 Particle composition from mass spectrometry

In Figure 6 we show speciated high-resolution mass spectra from the SP-AMS for nascent and thickly coated biomass-burning particles. The coating was SOA formed from α -pinene ozonolysis. High-resolution peak fitting was done using PIKA version 1.15 (Decarlo et al., 2006). Highly resolved ions were classified into a species and are displayed at unit mass resolution according to the fragmentation table therein. To account for C_1^+ that may result from the fragmentation of non-refractory OM components, the fragmentation table specifies that the amount of C_1^+ attributed to rBC is limited to $0.625 \cdot C_3^+$, the ratio observed for the rBC calibrant, Regal Black (Onasch et al., 2012). Recent studies have begun to investigate the degree to which non-refractory OM contributes to larger elemental-carbon ion fragments (C_x^+ , where $x > 1$) using IR laser vaporization. This has important implications for quantitative measurements of rBC using the SP-AMS and also for source apportionment based on the ion fragmentation pattern of rBC (Corbin et al., 2014).

We measured refractory and non-refractory material from nascent soot using the SP-AMS with the IR laser on. High-resolution analysis of non-refractory organic material showed significant contribution from aliphatic ions, $^{55}[C_4H_7]^+$, $^{57}[C_4H_9]^+$, $^{69}[C_5H_9]^+$, and $^{81}[C_6H_9]^+$. This is consistent with other AMS measurements of fresh, flaming-phase biomass-burning emissions (Corbin et al., 2015; Cubison et al., 2011; Hennigan et al., 2011). We also observed the highly oxygenated ions typically associated with levoglucosan, a common tracer for biomass-burning, $C_2H_3O_2^+$ ($m/z +60$) and $C_3H_5O_2^+$ ($m/z +73$). However, $C_2H_3O_2^+$ was less than 0.5% of the total organic signal for nascent soot, much less than what has previously been reported (Aiken et al., 2010; Corbin et al., 2015; Cubison et al., 2011; Hennigan et al., 2010, 2011; Lee et al., 2010). This is

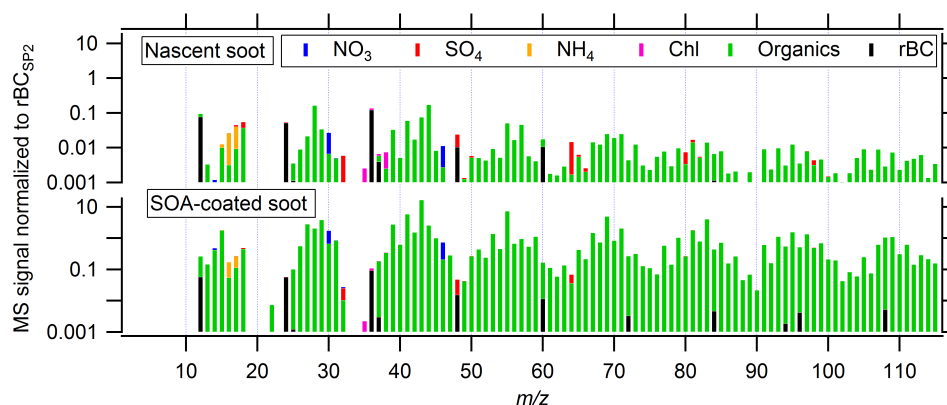


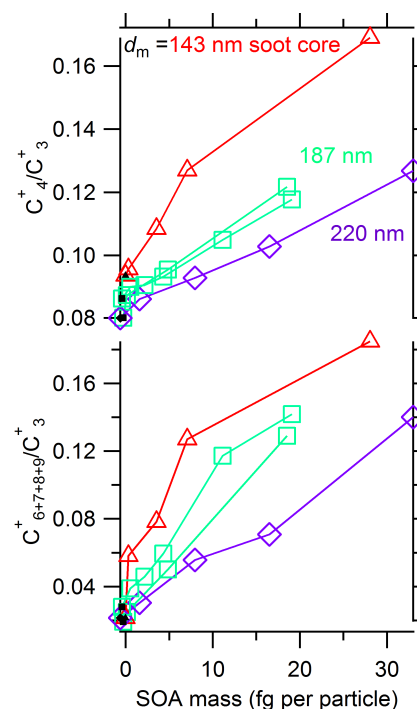
Figure 6. Stick integrated high-resolution mass spectra from the SP-AMS for nascent (top) and thickly SOA-coated soot (bottom). Mass spectra have been normalized by total rBC mass as measured by the SP2 to account for particle wall-loss. Peak bar colors correspond to the assigned chemical components for each unit m/z ion peak, based on analysis of the high-resolution mass spectra. The nascent soot spectrum is rich in refractory black carbon, inorganic ions, and organic fragments. The spectrum from the SOA-coated soot, on the other hand, is dominated by the OM from the secondary organic aerosol. However, increased sensitivity to larger EC fragments from rBC in the coated particles is obvious.

likely due to low cellulose content in the bark that we burned, resulting in less formation of the anhydrosugar levoglucosan compared to burning wood (Branca et al., 2007). The average oxidation state of carbon ($\overline{OS}_c = 2O:C - H:C$) for the organic fragments (including HO^+ , H_2O^+ , and CO_2^+) was -0.56 ± 0.25 . This low oxidation state is consistent with primary organic aerosol
5 (Canagaratna et al., 2014; Kroll et al., 2011). We also observed refractory material, including elemental carbon series ($C_1^+ - C_9^+$) and some metals including potassium, rubidium, and zinc. The alkali metals have very low ionization energies, and thus may become ionized by heating in the IR laser. This ionization mechanism is independent of the 70 eV electrons that usually ionize neutral vapors in the SP-AMS. A broad abnormal ion peak shape of the metals indicates that they underwent single-step thermal ionization in the IR beam, rather than conventional two-step thermal vaporization with subsequent electron ionization (Corbin et al., 2015; Drewnick et al., 2006).
10

Condensation of SOA from α -pinene ozonolysis increased the signal from most organic fragments. Especially notable was the signal increase for singly oxygenated organic fragments
15 $^{43}[C_2H_3O]^+$, $^{55}[C_3H_3O]^+$, $^{71}[C_4H_7O]^+$ and $^{83}[C_5H_7O]^+$. Reduced fragments such as $^{69}[C_5H_9]^+$ also increased with SOA coating. After a thick coating (with an SOA:BC mass ratio of approximately 9) the average oxidation state of carbon was 1.15 ± 0.04 . This is consistent with the α -pinene ozonolysis SOA formed in smog chambers (Chhabra et al., 2010; Shilling et al., 2008); however, the SOA mass spectra we obtain show relatively less fragmentation than similar α -pinene SOA mass spectra obtained with a conventional AMS using the 600 °C heater. This suggests that a significant fraction of the particles were vaporized by the IR laser ($> 97\%$ of the BBA contained sufficient black carbon that could be measured by the SP2) and that this produced marginally less fragmentation; the much lower f_{44} (fraction of total ion signal at $m/z +44$) is also consistent with this hypothesis.
20



Figure 7. SP-AMS measurements of carbon ion family (C_x^+) peak area ratios versus SOA coating mass on three different BBA soot-core sizes, indicated by symbol colors. SOA mass determined from SP-AMS measurements of all identified OM mass (as in Fig. 4). The ratio of C_4^+ and $C_{\Sigma 6-9}^+$ compared to C_3^+ , increases with organic coating either due to contributions to the C_x^+ family from non-refractory OM, and/or a decrease in relative fragmentation of EC to C_3^+ .



Attribution of rBC in the SP-AMS mass spectrum would be straightforward if graphitic material had a consistent fragmentation pattern and if all elemental carbon fragments (the C_x^+ family) arose only from rBC. However, neither is true. For instance, vaporized fullerenes have a different electron ionization C_x^+ fragmentation pattern than the Regal Black material we use as a calibrant (Onasch et al., 2015). It is well known that organic aerosol produces C_1^+ and C_2^+ fragments following electron ionization (Alfarra, 2004; Corbin et al., 2014), but we have evidence that SOA either produces larger C_x^+ fragments or that it changes the rBC fragmentation pattern. In Figure 7 we show the ion peak area ratios for C_4^+/C_3^+ and C_{6-9}^+/C_3^+ for size-selected soot particles as they became coated with SOA. The SOA mass per particle on the x-axis is the mass calculated from particle mobility measurements, described in section 2.3. Both ratios increase consistently with coating mass, with a larger slope for smaller cores (with smaller m_{rBC}). This is also apparent in Fig. 6, where black sticks representing EC from rBC are evident for $m/z \geq 72$ after SOA coating, while they were not detected in the nascent soot. Either the SOA coating changes the fragmentation pattern of EC to reduce the C_3^+ signal or the SOA generates significant signal for $C_{>3}^+$. This suggests that soot source apportionment by the SP-AMS might be most meaningful for rBC that has been thermally denuded to remove any coatings as this would remove any effect of OA on the C_x^+ ratios measured from the rBC.

We detected small amounts of non-refractory species other than OM, amounting to less than 10% of the total mass. Ammonium sulfate condensed onto the particles after they were injected into the chamber. This was probably caused by the formation of sulfuric acid from oxidation of $SO_{2(g)}$, and subsequent neutralization by ammonia in the dry chamber. We also detected nitrate ions after addition of ozone to the chamber, as well as after injections of α -



pinene, suggesting the formation of some organonitrates (Farmer et al., 2010; Zhang et al., 2006). The $\text{NO}^+/\text{NO}_2^+$ ratio was 2.2, as opposed to 1.45 for ammonium nitrate calibration particles. We observed chloride with both SP-AMS vaporizer modes (IR laser on and off), while the potassium signal was much larger when we operated the SP-AMS with the laser on. This is further evidence that the potassium is internally mixed with black carbon, and that it underwent one-step thermal ionization in the IR beam (Corbin et al., 2015; Drewnick et al., 2006; Lee et al., 2016). Sulfur dioxide, ammonia, nitrogen oxides, hydrogen chloride, and other chloride salts are known common primary emissions from biomass burning (Levin et al., 2010; Li et al., 2003; Reid et al., 2005; Stockwell et al., 2015; Zauscher et al., 2013).

Figure 8 shows single-polarity mass spectra obtained by the LAAPTOF for individual particles before and after coating with SOA. The characteristic ion series for elemental carbon included C_1^+ , C_2^+ , and C_3^+ . We also observed anions C_1^- and C_2^- for some particles, but not as consistently. We observed NO^+ in both coated and uncoated particles, as well as K^+ , readily identified by its isotopic abundance at m/z +39 and +41 (Bahadur et al., 2010; Healy et al., 2012; Silva et al., 1999). OM fragments tentatively identified as CO^+ at m/z +28 and $\text{C}_2\text{H}_3\text{O}^+$ at m/z +43 were measured from both nascent and oxidized particles. We also observed sulfur and sulfate ions (S^+ , SO^+ , and HSO_4^-), likely fragments of sulfates. Zn^+ was observed and identified by its isotopic fingerprint.

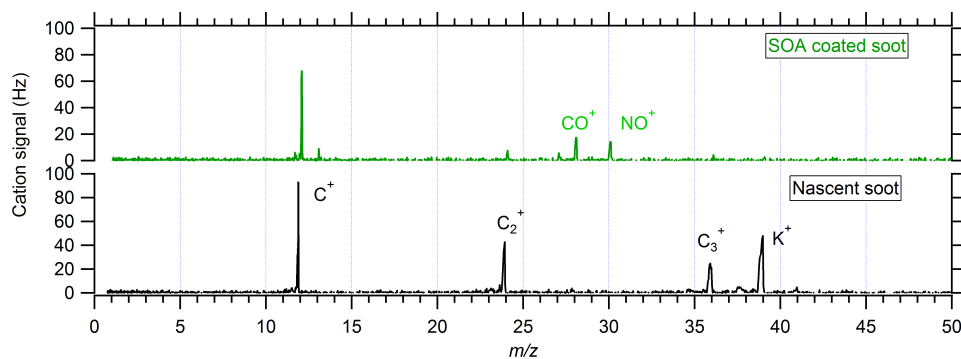


Figure 8. Positive polarity mass spectra and ion assignments for two representative particles analyzed by the LAAPTOF. The elemental carbon fragment series (C_x^+) dominates the nascent soot spectra in the bottom, while the contribution from oxidized organic matter is increased in the top panel for a soot particle that was coated with α -pinene SOA.

3.3 SP-AMS sensitivity to refractory species

We determined the ion response of the SP-AMS to biomass-burning particles as a function of SOA coating mass using two ions produced from refractory biomass-burning material – K^+ and C_3^+ – normalized by the rBC mass concentration measured by the SP2 (rBC_{SP2}). In Figure 9 we show the K^+ and C_3^+ SP-AMS ion signal per rBC_{SP2} mass during progressive SOA coating experiments. The plotted points are ten-minute averages for four batch chamber experiments using different initial soot core sizes. We determined the SOA mass per particle using the method described in section 2.3. Different colored and shaped traces indicate the mobility mode diameter of the initial soot core injected into the chamber, and the black dots indicate the initial nascent soot, prior to SOA coating. We used the SP2-measured BC mass to

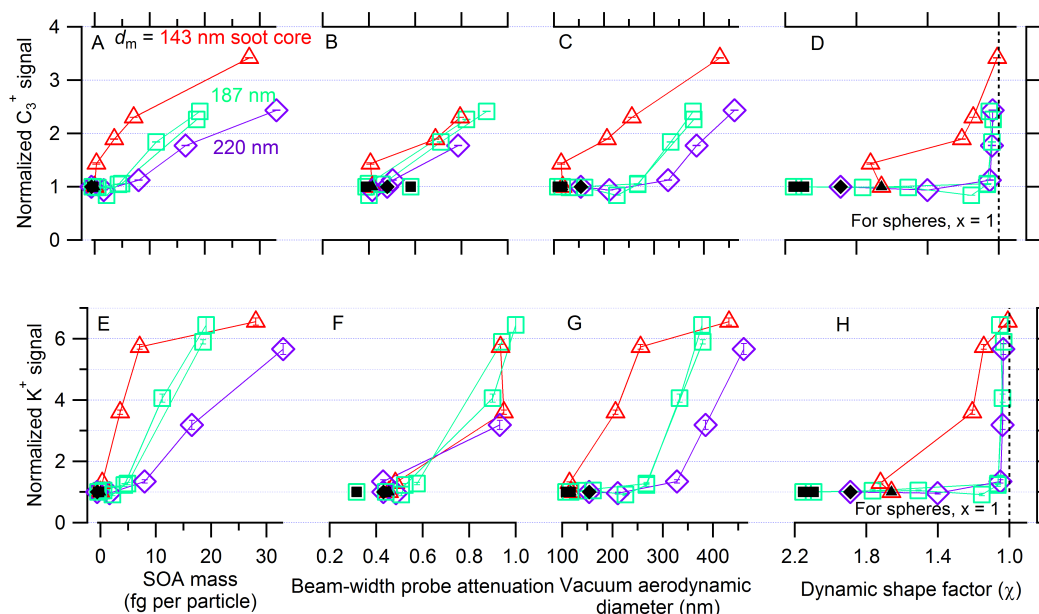


Figure 9. SP-AMS-measured biomass-burning ion signals for C_3^+ (top) and K^+ (bottom) for three mobility selected core particle sizes versus four different metrics. These signals are corrected for particle wall-loss using SP2-measured rBC, and then normalized to values obtained from the uncoated nascent soot. Symbols are colored/shaped by their initial soot core mobility diameter, prior to SOA coating, where red triangles = 143 nm, teal squares = 187 nm (two replicate experiments), and purple diamonds = 220 nm. The nascent particles are indicated by black dots, and the lines connect them with the data points following subsequent SOA coatings. The left panels (a and e) display the normalized ratio of the SP-AMS-measured C_3^+ and K^+ ion signals, respectively, to the SP2-measured black carbon mass concentration as a function of the mass of SOA per particle. The SP-AMS:SP2 ratio is normalized to the uncoated soot values. Panels (b and f) display the attenuation of the SP-AMS ion signal caused by the beam-width probe in the center of the particle beam; greater attenuation indicates a more collimated, narrow particle beam, as expected for particles that are larger and/or more spherical. Panels (c and g) display the mode mobility diameter of the particles that produced either the C_3^+ or K^+ ion signal. Panels (e and h) display the particle dynamic shape factor; particles start as less spherical ($\chi > 1.0$) and move towards sphericity ($\chi = 1$) as more SOA mass is added. The measurement uncertainties are indicated by the vertical error bars and represent the standard deviation of one-minute AMS integration time from the ten-minute averages presented by each symbol.

correct for particle wall loss in the chamber because the rBC mass measurement of the SP2 is insensitive to particle shape and coating thickness for particles with at least 0.7 fg of rBC present (Schwarz et al., 2010). The smallest particle mode measured in these experiments was 1.1 fg of BC, well above detection limits for the SP2.

- 5 Potassium is a useful marker for refractory BBA material because it has a high signal-to-noise ratio, it is not produced by fragmentation of non-refractory OM, and it is a non-volatile unreactive conserved tracer. By turning off the IR laser we confirmed that very little of the potassium signal resulted from particles that hit the conventional 600 °C heater (< 1% of total K^+ signal with IR laser on). Therefore, the potassium we observed with the IR laser on was



internally mixed with rBC. We selected C_3^+ at m/z 36 as an ion of interest because of its large contribution to the total rBC C_x^+ family signal (Fig. 4), and the very low contribution from OM. The C_3^+ signal from OM is less than 0.08% of the total OM signal when the IR laser is off and particles are vaporized by the heater. One important difference between the two measured species, K^+ and C_3^+ , is the method of ion formation within the SP-AMS. rBC undergoes the conventional process of IR vaporization followed by 70 eV electron ionization of neutral vapors. Potassium, however, has a very low ionization energy and at high temperatures can undergo one-step, thermal ionization, without interacting with 70 eV electrons to become ionized (Corbin et al., 2015; Drewnick et al., 2006; Svane et al., 2004; Zandberg, 1995). Furthermore, rBC particles approach ~ 4000 K in the IR laser before vaporizing, while potassium may vaporize/ionize at temperatures less than 1500 K (Svane et al., 2004).

Panels (a) and (e) in Fig. 9 reveal an increasing SP-AMS response to both potassium and rBC as the SOA coating grew. Panels (b) and (f) show the attenuation of the K^+ or C_3^+ ion signal normalized to SP2-measured rBC, with the beam-width probe placed in the center of the particle beam. The attenuation increased as the SOA coating thickened because the particle beam narrowed. The increased response of the SP-AMS with successive coatings of SOA is thus due to an increase in the SP-AMS IR-beam particle collection efficiency, E_s . However, the attenuation of K^+ rises steeply, whereas the attenuation of C_3^+ steadily continues to rise more shallowly with coating thickness.

The IR laser beam waist that vaporizes particles has a roughly Gaussian intensity profile. The difference we observe between C_3^+ and K^+ attenuation suggests that the effective IR beam for vaporizing rBC, described by Willis et al. (2014), is narrower than the effective beam for thermal ionization of potassium. That is, rBC must pass through a region of higher laser energy density near the center of the IR beam to be vaporized, ionized by the electron source, and then detected than is required for thermal ionization of potassium. If an internally mixed particle containing potassium and rBC passes through the center of the laser, two processes will take place. rBC will become vaporized and ionized, and potassium will be thermally ionized. However, our measurements show that particles may pass through the potassium thermal ionization region of the IR beam but miss the smaller rBC vaporization region.

The ability of an aerodynamic lens, such as that used on the SP-AMS, to effectively focus a particle depends on two parameters: the particle size and also the particle shape. Panels (c) and (g) in Fig. 9 illustrate the increasing response of the SP-AMS to coated rBC as a function of vacuum aerodynamic diameter. The particles grow as more SOA mass is condensed, and the larger particles are focused more efficiently by the aerodynamic lens towards the center of the IR laser, resulting in a larger instrument ion signal response with both increasing particle size and increasing SOA mass. The other factor that influences effective focusing of the particles in an aerodynamic lens is particle shape, reported as a calculated dynamic shape factor, χ . As seen in panels (d) and (h), the shape factor decreases towards unity ($\chi = 1$ for spheres) as the particles become more thickly coated with SOA. Although the particles become nearly spherical after a few coatings, they still need to grow to a sufficiently large diameter to be successfully focused into the IR laser beam of the SP-AMS. Neither particle shape nor diameter alone is sufficient to describe E_s . Even at $d_{va} = 250$ nm there is a factor of two difference in response to particles with different dynamic shape factors. However, the largest increase in instrument response occurs after the particles are mostly spherical ($\chi < 1.2$), which as we discussed in section 2.3 may

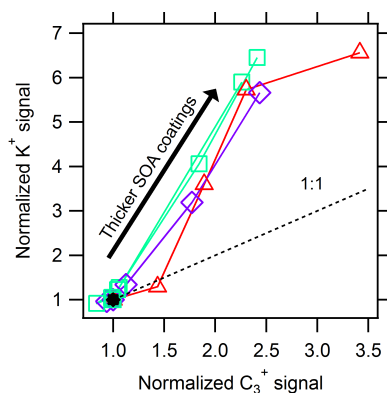


Figure 10. Correlation of refractory ion signals from the SP-AMS during SOA coating experiments. Colored symbols represent the relative enhancement of K^+ and C_3^+ , as in Fig. 9. All four traces, indicating different coating experiments, begin at (1,1) and generally increase with increasing SOA coating. The increase in measured K^+ compared to C_3^+ ion signal for the same coatings shows that there are two different effective laser widths for the processes, thermal ionization of K^+ and two-step vaporization-ionization of rBC, respectively.

describe the state of rBC particles in ambient biomass burning plumes after less than 1 hour of aging. This increase in instrument signal is driven by growth from condensation of additional SOA. Panels (d) and (h) demonstrate this by plotting the refractory ion signal ratios versus the dynamic shape factor (χ) calculated as described in section 2.3.

5 Figure 10 shows the same normalized K^+ and C_3^+ signals from Fig. 9, accounting for
particle wall-loss and normalized to the ion response under nascent conditions. The differently
shaped and colored traces show the relative enhancement of ion signals, measured for the same
SOA coating conditions. The greater increase in the K^+ signal compared to the increase in the
10 C_3^+ ion signal for the same coatings is attributed to two distinct ion formation mechanisms that
the two species experienced. As the IR laser has a Gaussian intensity profile, the different
mechanisms occur in different regions of the IR beam. Evidently, a higher intensity is necessary
for the vaporization of rBC, but a lower intensity can still drive thermal vaporization/ionization
of alkali metals, such as potassium and sodium. The Gaussian IR beam thus has a greater
effective width for alkali metals than for rBC.

15 Figure 11 displays the wall-loss corrected K^+ and C_x^+ signal measured by the SP-AMS
as a function of wall-loss corrected OM signal. We corrected the SP-AMS signal for wall losses
using the rBC mass measurement from the SP2, and we normalized the signals from each
experiment to the signals for the nascent soot particles. We smoothed the traces using a 3-point
20 boxcar moving average to clarify trends. The OM signal is not quantitative due to unknown
relative ionization and collection efficiencies for organics detected with both the IR laser and
heater operating simultaneously. However, it provides a high time resolution relative metric of
the amount of condensed SOA. It shows that even at our highest achieved coating thickness the
signals from both K^+ and C_x^+ continued to increase; neither signal saturated. This illustrates that
particle beam width is an important metric for quantitative measurements of BBA, even with a
25 high SOA:rBC mass ratio > 9 , and particle vacuum aerodynamic diameters greater than 400 nm.

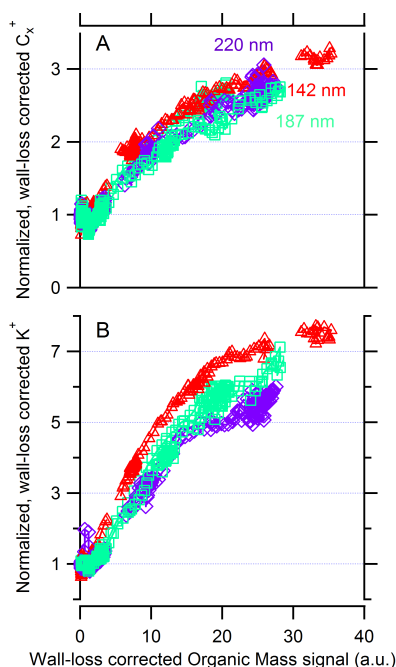


Figure 11. Wall-loss corrected SP-AMS signal from rBC C_x^+ (panel A) and K^+ (panel B) have been normalized to their nascent values (before SOA coating) and are shown as a function of wall-loss corrected SP-AMS OM signal. Marker shapes and sizes indicate the initial soot core mobility diameter for a given experiment. One-minute averages show that the evolution of the particle sensitivity is continuous, and that even at our thickest SOA coating, we continue to see an increase in instrument sensitivity to both rBC and K refractory material.

3.4 LAAPTOF quantification of OM on externally mixed soot particles

We show the average OM signal per particle measured by the LAAPTOF in Fig. 12. We observed a large degree of molecular fragmentation; most of the OM signal appeared at m/z +28, which we attribute to CO^+ . All data points represent the average of at least five particles with a minimum of 100 Hz of total EC ion signal at m/z +24, +36, +48, and +60, representing C_2 - 5^+ . This excludes any homogeneously nucleated SOA particles and low-signal particles from the analysis. A linear regression fit of all LAAPTOF OM ion signal as a function of SOA mass per particle results in a $R^2 = 0.72$ (OM signal (Hz) = $75(\text{fg SOA}) + 167$). This may be due to different light absorption and laser energy distribution properties of different sized soot cores.

5
10

Narrowing the analysis to the experiment with 187 nm soot cores results in a highly linear fit with a $R^2 = 0.998$ (OM signal (Hz) = $120(\text{fg SOA}) + 179$). Despite the complex nature of the SOA coating and biomass-burning aerosol core, we observed a strong linear relationship between the amount of SOA condensed on the particle and the OM signal from the LAAPTOF.

Figure 13 shows the same OM ion signal measured by the LAAPTOF plotted in Figure 12, now normalized by the concurrent LAAPTOF EC ion signal. This parallels the analysis by ATOFMS of spark-generated EC particles coated by the condensation of diesel fuel presented

15

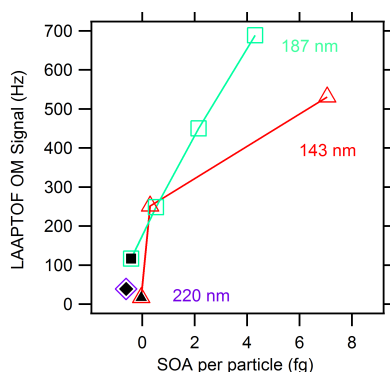


Figure 12. Averaged OM signal ($m/z +28$; CO^+) from nascent and SOA-coated soot particles measured by the LAAPTOF during SOA coating experiments vs. SOA mass per particle. There is a strong positive correlation despite the complex biomass-burning aerosol matrix. Open marker colors/shapes indicate the initial d_{mob} of the size-selected soot core, and black markers indicate nascent, uncoated soot particles.

by Spencer and Prather (2006), but using more complex and realistic particle EC and OM components. EC fragments used included C_{2-5}^+ but excluded C_1^+ because we have observed that OM can also be charred to C_1^+ and thus produce an interference to the quantification of EC at $m/z 12$. The OM:EC ion ratio used here is thus $\text{CO}^+:\text{C}_{2-5}^+$. We use the ratio of OM/EC ions to account for laser shot-to-shot variability, where more ions may be generated due to increased laser fluence or increased absorption of laser energy. We sampled biomass-burning particles that contained potassium salts, which ionize readily, as well as strongly light-absorbing rBC (Gross et al., 2000). This represents the complex composition of realistic aged BBA. Despite the variability in the soot core composition of individual particles, a strong linear relationship between the amount of SOA mass per particle and the LAAPTOF ion signal from oxidized organics is still observed from these mixed rBC and inorganic salt particles, when averaged over

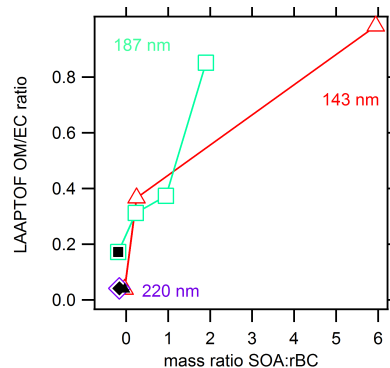


Figure 13. LAAPTOF-measured OM ion signal ($m/z +28$; CO^+) normalized by LAAPTOF EC ion signal (sum of $m/z +24$, $+36$, $+48$, $+60$; C_{2-5}^+) for uncoated and SOA coated soot particles. Here the OM:EC ratio is shown as a function of the ratio of mobility-derived SOA mass to SP2-measured rBC. The LAAPTOF EC signal serves as an internal standard to normalize for the actual amount of laser energy the particle absorbed, which can change with increased rBC mass or SOA coating, and particle size and shape. Marker colors/shapes indicate the initial size-selected soot core d_{mob} for each experiment.



the many particles we sampled.

Other LDI-SP-MS instruments that use longer ionization wavelengths, such as 266 nm used in the ATOFMS, do not typically fragment oxidized organics to CO^+ ; instead their major oxidized OM ion fragment is observed at $m/z +43$, presumably from $\text{C}_2\text{H}_3\text{O}^+$ (Moffet and Prather, 2009; Spencer and Prather, 2006). We operated the LAAPTOF's excimer laser at a moderate pulse energy of 2.0 mJ, as a tradeoff between increased sensitivity while avoiding excessive charring or fragmentation of OM into EC C_n^+ fragments. In the work described in Spencer and Prather (2006), graphitic soot particles with no condensed organics had an OM:EC ion signal ratio of ~ 0 , and those coated with a mass of condensed fuel equal to the EC mass had an OM:EC ion signal ratio of 2.25. For a similar OM:EC mass ratio ~ 1 in our experiments, we saw a more modest LAAPTOF OM:EC ratio of ~ 0.35 . This difference may be caused by differences in instrument operation and chemical composition of the refractory EC core and OM coating. The LAAPTOF uses an exciplex VUV laser at 193 nm (compared to the "softer" 266 nm Nd:YAG laser in the ATOFMS) and we observe more extensive molecular fragmentation of the OM. Thus, we quantified OM with a single ion (CO^+), compared to the various ions used by Spencer and Prather (i.e. $m/z +27, +29, +37, +43$). A softer ionization might have resulted in less charring of SOA to C_1^+ in the LAAPTOF, and thus increased the slope of the LAAPTOF-measured OM:EC ions versus mass fraction of SOA. Spencer and Prather used condensed diesel fuel vapors as their source of OM, while we used SOA from the ozonolysis of α -pinene. Therefore, the OM used in the prior study was unoxidized primary organic aerosol, while our OM was highly oxidized complex secondary organic aerosol.

4 Conclusions

We investigated the response of two particle mass spectrometers to biomass-burning particles with carefully controlled amounts of organic matter and well characterized particle properties. Our analysis revealed a variety of particle morphologies and compositions, leading to a broad distribution of vacuum aerodynamic diameters at a single selected mobility diameter. As these particles of various compositions and shapes became coated with SOA, measurements using the beam-width probe of the SP-AMS revealed that the effective IR laser beam width for thermal ionization of potassium is larger than for vaporization of rBC. Although these measurements explored thick SOA coatings and large particle sizes, we did not observe a plateau in instrument response to potassium or black carbon as the coating was increased. These findings have important implications for obtaining quantitative mass measurements, and can help to better inform the analysis and interpretation of SP-AMS measurements of the emissions and aging biomass-burning aerosol (Lee et al., 2016).

Mass spectral analysis with the SP-AMS also revealed that increased SOA coatings on the biomass-burning soot changed the relative abundance of elemental-carbon clusters. Specifically, as the particles became more thickly coated with SOA, the ratio of $\text{C}_{\Sigma 6-9}^+$ to C_3^+ increased. The degree of change is smaller than the precision suggested Corbin et al. (2014) for identifying soot-particle source types using ratios of the elemental-carbon ion family, C_x^+ . However, contrary to Corbin et al. (2014), we did not observe the characteristic fullerene-rich signal they previously reported for fuel-rich combustion.

Despite the challenges presented by complex particle composition and shape for laser desorption ionization single-particle mass spectrometry, there is a strong correlation between



the average OM ion signal measured by the LAAPTOF and the SOA mass per particle. Although this quantitative relationship has been shown previously for LDI-SP-MS analysis of graphite spark discharge soot coated by diesel fuel condensation (Spencer and Prather, 2006), this is the first time it has been explored with realistic combustion soot in the presence of

5 inorganic components and complex realistic SOA. This opens the way for more quantitative single-particle measurements using techniques such as laser-beam homogenization and particle type informed ion sensitivity calibrations. Additional work is required to investigate the response of single-particle mass spectrometry to other atmospherically relevant core-shell combinations.

10 Acknowledgements

AA and GS were partially supported by the Steinbrenner Graduate Research Fellowship. R. Subramanian was funded by the US Department of Energy Atmospheric Systems Research program through grant DE- SC0010121. The authors thank Claudio Mazzoleni for the loan of the CPMA. The views, opinions, and/or findings contained in this paper are those of the

15 authors and should not be construed as an official position of the funding agencies.

References

- Aiken, A. C., de Foy, B., Wiedinmyer, C., DeCarlo, P. F., Ulbrich, I. M., Wehrli, M. N., Szidat, S., Prevot, A. S. H., Noda, J., Wacker, L., Volkamer, R., Fortner, E., Wang, J., Laskin, A., Shutthanandan, V., Zheng, J., Zhang, R., Paredes-Miranda, G., Arnott, W. P., Molina, L. T., Sosa, G., Querol, X. and Jimenez, J. L.: Mexico city aerosol analysis during MILAGRO using high resolution aerosol mass spectrometry at the urban supersite (T0) – Part 2: Analysis of the biomass burning contribution and the non-fossil carbon fraction, *Atmos. Chem. Phys.*, 10(12), 5315–5341, doi:10.5194/acp-10-5315-2010, 2010.
- Alfarra, M. R.: Insights Into Atmospheric Organic Aerosols Using An Aerosol Mass Spectrometer, University of Manchester, 2004.
- 25 Andreae, M. O.: Soot carbon and excess fine potassium: long-range transport of combustion-derived aerosols., *Science*, 220(4602), 1148–51, doi:10.1126/science.220.4602.1148, 1983.
- Anenberg, S. C., Schwartz, J., Shindell, D., Amann, M., Faluvegi, G., Klimont, Z., Janssens-Maenhout, G., Pozzoli, L., Van Dingenen, R., Vignati, E., Emberson, L., Muller, N. Z., West, J. J., Williams, M., Demkine, V., Hicks, W. K., Kuylenstierna, J., Raes, F. and Ramanathan, V.: Global Air Quality and Health Co-
- 30 benefits of Mitigating Near-Term Climate Change through Methane and Black Carbon Emission Controls, *Environ. Health Perspect.*, 120(6), 831–839, doi:10.1289/ehp.1104301, 2012.
- Bahadur, R., Russell, L. M. and Prather, K. A.: Composition and Morphology of Individual Combustion, Biomass Burning, and Secondary Organic Particle Types Obtained Using Urban and Coastal ATOFMS and STXM-NEXAFS Measurements, *Aerosol Sci. Technol.*, 44(7), 551–562, doi:10.1080/02786821003786048, 2010.
- 35 Bhave, P. V., Allen, J. O., Morrical, B. D., Fergenson, D. P., Cass, G. R. and Prather, K. A.: A Field-Based Approach for Determining ATOFMS Instrument Sensitivities to Ammonium and Nitrate, *Environ. Sci. Technol.*, 36(22), 4868–4879, doi:10.1021/es015823i, 2002.
- Bond, T. C., Doherty, S. J., Fahey, D. W., Forster, P. M., Berntsen, T., DeAngelo, B. J., Flanner, M. G., Ghan, S., Kärcher, B., Koch, D., Kinne, S., Kondo, Y., Quinn, P. K., Sarofim, M. C., Schultz, M. G., Schulz, M., Venkataraman, C., Zhang, H., Zhang, S., Bellouin, N., Guttikunda, S. K., Hopke, P. K., Jacobson, M. Z., Kaiser, J. W., Klimont, Z., Lohmann, U., Schwarz, J. P., Shindell, D., Storelvmo, T., Warren, S. G. and Zender, C. S.: Bounding the role of black carbon in the climate system: A scientific assessment, *J. Geophys. Res. Atmos.*, 118(11), 5380–5552, doi:10.1002/jgrd.50171, 2013.
- 45 Branca, C., Iannace, A. and Di Blasi, C.: Devolatilization and Combustion Kinetics of *Quercus cerris* Bark,



- Energy & Fuels, 21(2), 1078–1084, doi:10.1021/ef060537j, 2007.
- Canagaratna, M. R., Jimenez, J. L., Kroll, J. H., Chen, Q., Kessler, S. H., Massoli, P., Hildebrandt Ruiz, L., Fortner, E., Williams, L. R., Wilson, K. R., Surratt, J. D., Donahue, N. M., Jayne, J. T. and Worsnop, D. R.: Elemental ratio measurements of organic compounds using aerosol mass spectrometry: characterization, improved calibration, and implications, *Atmos. Chem. Phys.*, 14(13), 19791–19835, doi:10.5194/acpd-14-19791-2014, 2014.
- 5 Chen, K., Yin, Y., Kong, S., Xiao, H., Wu, Y., Chen, J. and Li, A.: Size-resolved chemical composition of atmospheric particles during a straw burning period at Mt. Huang (the Yellow Mountain) of China, *Atmos. Environ.*, 84, 380–389, doi:10.1016/j.atmosenv.2013.11.040, 2014.
- 10 Chhabra, P. S., Flagan, R. C. and Seinfeld, J. H.: Elemental analysis of chamber organic aerosol using an aerodyne high-resolution aerosol mass spectrometer, *Atmos. Chem. Phys.*, 10(9), 4111–4131, doi:10.5194/acp-10-4111-2010, 2010.
- Chung, S. H.: Global distribution and climate forcing of carbonaceous aerosols, *J. Geophys. Res.*, 107(D19), 4407, doi:10.1029/2001JD001397, 2002.
- 15 Corbin, J. C., Sierau, B., Gysel, M., Laborde, M., Keller, A., Kim, J., Petzold, A., Onasch, T. B., Lohmann, U. and Mensah, A. A.: Mass spectrometry of refractory black carbon particles from six sources: Carbon-cluster and oxygenated ions, *Atmos. Chem. Phys.*, 14(5), 2591–2603, doi:10.5194/acp-14-2591-2014, 2014.
- Corbin, J. C., Lohmann, U., Sierau, B., Keller, A., Burtscher, H. and Mensah, A. A.: Black-carbon-surface oxidation and organic composition of beech-wood soot aerosols, *Atmos. Chem. Phys. Discuss.*, 15(6), 9573–9629, doi:10.5194/acpd-15-9573-2015, 2015.
- 20 Cubison, M. J., Ortega, A. M., Hayes, P. L., Farmer, D. K., Day, D., Lechner, M. J., Brune, W. H., Apel, E., Diskin, G. S., Fisher, J. A., Fuelberg, H. E., Hecobian, A., Knapp, D. J., Mikoviny, T., Riemer, D., Sachse, G. W., Sessions, W., Weber, R. J., Weinheimer, A. J., Wisthaler, A. and Jimenez, J. L.: Effects of aging on organic aerosol from open biomass burning smoke in aircraft and laboratory studies, *Atmos. Chem. Phys.*, 11(23), 12049–12064, doi:10.5194/acp-11-12049-2011, 2011.
- 25 DeCarlo, P. F., Slowik, J. G., Worsnop, D. R., Davidovits, P. and Jimenez, J. L.: Particle Morphology and Density Characterization by Combined Mobility and Aerodynamic Diameter Measurements. Part 1: Theory, *Aerosol Sci. Technol.*, 38(12), 1185–1205, doi:10.1080/027868290903907, 2004.
- Decarlo, P. F., Kimmel, J. R., Trimborn, A., Northway, M. J., Jayne, J. T., Aiken, A. C., Gonin, M., Fuhrer, K., Horvath, T., Docherty, K. S., Worsnop, D. R. and Jimenez, J. L.: Field-deployable, high-resolution, time-of-flight aerosol mass spectrometer, *Anal. Chem.*, 78(24), 8281–8289, doi:10.1021/2001JD001213, 2006.
- 30 Drewnick, F., Hings, S. S., Curtius, J., Eerdekens, G. and Williams, J.: Measurement of fine particulate and gas-phase species during the New Year's fireworks 2005 in Mainz, Germany, *Atmos. Environ.*, 40(23), 4316–4327, doi:10.1016/j.atmosenv.2006.03.040, 2006.
- 35 Farmer, D. K. and Jimenez, J. L.: Real-time Atmospheric Chemistry Field Instrumentation †, *Anal. Chem.*, 82(19), 7879–7884, doi:10.1021/ac1010603, 2010.
- Farmer, D. K., Matsunaga, A., Docherty, K. S., Surratt, J. D., Seinfeld, J. H., Ziemann, P. J. and Jimenez, J. L.: Response of an aerosol mass spectrometer to organonitrates and organosulfates and implications for atmospheric chemistry, *Proc. Natl. Acad. Sci.*, 107(15), 6670–6675, doi:10.1073/pnas.0912340107, 2010.
- 40 Ferguson, D. P., Song, X.-H., Ramadan, Z., Allen, J. O., Hughes, L. S., Cass, G. R., Hopke, P. K. and Prather, K. A.: Quantification of ATOFMS Data by Multivariate Methods, *Anal. Chem.*, 73(15), 3535–3541, doi:10.1021/ac010022j, 2001.
- 45 Gemayel, R., Hellebust, S., Temime-Roussel, B., Hayeck, N., Van Elteren, J. T., Wortham, H. and Gligorovski, S.: The performance and the characterization of laser ablation aerosol particle time-of-flight mass spectrometry (LAAP-ToF-MS), *Atmos. Meas. Tech.*, 9(4), 1947–1959, doi:10.5194/amt-9-1947-2016, 2016.



- Gross, D. S., Gälli, M. E., Silva, P. J. and Prather, K. A.: Relative Sensitivity Factors for Alkali Metal and Ammonium Cations in Single-Particle Aerosol Time-of-Flight Mass Spectra, *Anal. Chem.*, 72(2), 416–422, doi:10.1021/ac990434g, 2000.
- 5 Gysel, M., Laborde, M., Olfert, J. S., Subramanian, R. and Gréhn, A. J.: Effective density of Aquadag and fullerene soot black carbon reference materials used for SP2 calibration, *Atmos. Meas. Tech.*, 4(12), 2851–2858, doi:10.5194/amt-4-2851-2011, 2011.
- Healy, R. M., Sciare, J., Poulain, L., Kamili, K., Merkel, M., Müller, T., Wiedensohler, A., Eckhardt, S., Stohl, A., Sarda-Estève, R., McGillicuddy, E., O'Connor, I. P., Sodeau, J. R. and Wenger, J. C.: Sources and mixing state of size-resolved elemental carbon particles in a European megacity: Paris, *Atmos. Chem. Phys.*, 12(4), 1681–1700, doi:10.5194/acp-12-1681-2012, 2012.
- 10 Healy, R. M., Sciare, J., Poulain, L., Crippa, M., Wiedensohler, A., Prévôt, a. S. H., Baltensperger, U., Sarda-Estève, R., McGuire, M. L., Jeong, C.-H., McGillicuddy, E., O'Connor, I. P., Sodeau, J. R., Evans, G. J. and Wenger, J. C.: Quantitative determination of carbonaceous particle mixing state in Paris using single particle mass spectrometer and aerosol mass spectrometer measurements, *Atmos. Chem. Phys. Discuss.*, 13(4), 10345–10393, doi:10.5194/acpd-13-10345-2013, 2013.
- 15 Hennigan, C. J., Sullivan, A. P., Collett, J. L. and Robinson, A. L.: Levoglucosan stability in biomass burning particles exposed to hydroxyl radicals, *Geophys. Res. Lett.*, 37(9), 2–5, doi:10.1029/2010GL043088, 2010.
- Hennigan, C. J., Miracolo, M. A., Engelhart, G. J., May, A. A., Presto, A. A., Lee, T., Sullivan, A. P., McMeeking, G. R., Coe, H., Wold, C. E., Hao, W.-M., Gilman, J. B., Kuster, W. C., de Gouw, J. A., Schichtel, B. A., Kreidenweis, S. M. and Robinson, A. L.: Chemical and physical transformations of organic aerosol from the photo-oxidation of open biomass burning emissions in an environmental chamber, *Atmos. Chem. Phys.*, 11(15), 7669–7686, doi:10.5194/acp-11-7669-2011, 2011.
- 20 Huffman, J. A., Jayne, J. T., Drewnick, F., Aiken, A. C., Onasch, T., Worsnop, D. R. and Jimenez, J. L.: Design, Modeling, Optimization, and Experimental Tests of a Particle Beam Width Probe for the Aerodyne Aerosol Mass Spectrometer, *Aerosol Sci. Technol.*, 39(12), 1143–1163, doi:10.1080/02786820500423782, 2005.
- Jacobson, M. Z.: Strong radiative heating due to the mixing state of black carbon in atmospheric aerosols, *Nature*, 409(6821), 695–697, doi:10.1038/35055518, 2001.
- 30 Jayne, J. T., Leard, D. C., Zhang, X., Davidovits, P., Smith, K. A., Kolb, C. E. and Worsnop, D. R.: Development of an Aerosol Mass Spectrometer for Size and Composition Analysis of Submicron Particles, *Aerosol Sci. Technol.*, 33(1-2), 49–70, doi:10.1080/027868200410840, 2000.
- Jeong, C.-H., McGuire, M. L., Godri, K. J., Slowik, J. G., Rehbein, P. J. G. and Evans, G. J.: Quantification of aerosol chemical composition using continuous single particle measurements, *Atmos. Chem. Phys.*, 11(14), 7027–7044, doi:10.5194/acp-11-7027-2011, 2011.
- 35 Kroll, J. H., Donahue, N. M., Jimenez, J. L., Kessler, S. H., Canagaratna, M. R., Wilson, K. R., Altieri, K. E., Mazzoleni, L. R., Wozniak, A. S., Bluhm, H., Mysak, E. R., Smith, J. D., Kolb, C. E. and Worsnop, D. R.: Carbon oxidation state as a metric for describing the chemistry of atmospheric organic aerosol, *Nat. Chem.*, 3(2), 133–139, doi:10.1038/nchem.948, 2011.
- 40 Lack, D. A., Cappa, C. D., Cross, E. S., Massoli, P., Ahern, A. T., Davidovits, P. and Onasch, T. B.: Absorption Enhancement of Coated Absorbing Aerosols: Validation of the Photo-Acoustic Technique for Measuring the Enhancement, *Aerosol Sci. Technol.*, 43(10), 1006–1012, doi:10.1080/02786820903117932, 2009.
- 45 Lee, A. K. Y., Willis, M. D., Healy, R. M., Wang, J. M., Jeong, C.-H., Wenger, J. C., Evans, G. J. and Abbatt, J. P. D.: Single-particle characterization of biomass burning organic aerosol (BBOA): evidence for non-uniform mixing of high molecular weight organics and potassium, *Atmos. Chem. Phys.*, 16(9), 5561–5572, doi:10.5194/acp-16-5561-2016, 2016.
- Lee, T., Sullivan, A. P., Mack, L., Jimenez, J. L., Kreidenweis, S. M., Onasch, T. B., Worsnop, D. R., Malm,



- W., Wold, C. E., Hao, W. M. and Collett, J. L.: Chemical Smoke Marker Emissions During Flaming and Smoldering Phases of Laboratory Open Burning of Wildland Fuels, *Aerosol Sci. Technol.*, 44(9), i–v, doi:10.1080/02786826.2010.499884, 2010.
- 5 Levin, E. J. T., McMeeking, G. R., Carrico, C. M., Mack, L. E., Kreidenweis, S. M., Wold, C. E., Moosmüller, H., Arnott, W. P., Hao, W. M., Collett, J. L. and Malm, W. C.: Biomass burning smoke aerosol properties measured during Fire Laboratory at Missoula Experiments (FLAME), *J. Geophys. Res.*, 115(D18), 1–15, doi:10.1029/2009JD013601, 2010.
- 10 Li, J., Posfai, M., Hobbs, P. V. and Buseck, P. R.: Individual Aerosol Particles from Biomass Burning in Southern Africa Compositions and Aging of Inorganic Particles, , 108, 1–12, doi:10.1029/2002JD002310, 2003.
- Liu, P., Ziemann, P. J., Kittelson, D. B. and McMurry, P. H.: Generating Particle Beams of Controlled Dimensions and Divergence: II. Experimental Evaluation of Particle Motion in Aerodynamic Lenses and Nozzle Expansions, *Aerosol Sci. Technol.*, 22(3), 314–324, doi:10.1080/02786829408959749, 1995.
- 15 Mansoori, B. A., Johnston, M. V. and Wexler, A. S.: Quantitation of Ionic Species in Single Microdroplets by On-Line Laser Desorption/Ionization, , 66(21), 3681–3687, 1994.
- Mansoori, B. A., Johnston, M. V. and Wexler, A. S.: Matrix-Assisted Laser Desorption/Ionization of Size- and Composition-Selected Aerosol Particles, *Anal. Chem.*, 68(20), 3595–3601, doi:10.1021/ac9603385, 1996.
- 20 Marsden, N., Flynn, M. J., Taylor, J. W., Allan, J. D. and Coe, H.: Evaluating the influence of laser wavelength and detection stage geometry on optical detection efficiency in a single particle mass spectrometer, *Atmos. Meas. Tech. Discuss.*, 1–25, doi:10.5194/amt-2016-150, 2016.
- May, A. A., Levin, E. J. T., Hennigan, C. J., Riipinen, I., Lee, T., Collett, J. L., Jimenez, J. L., Kreidenweis, S. M. and Robinson, A. L.: Gas-particle partitioning of primary organic aerosol emissions: 3. Biomass burning, *J. Geophys. Res. Atmos.*, 118(19), 11,327–11,338, doi:10.1002/jgrd.50828, 2013.
- 25 Mikhailov, E. F., Vlasenko, S. S., Podgorny, I. A., Ramanathan, V. and Corrigan, C. E.: Optical properties of soot-water drop agglomerates: An experimental study, *J. Geophys. Res.*, 111(D7), D07209, doi:10.1029/2005JD006389, 2006.
- Moffet, R. C. and Prather, K. A.: In-situ measurements of the mixing state and optical properties of soot with implications for radiative forcing estimates, *Proc. Natl. Acad. Sci.*, 106(29), 11872–11877, doi:10.1073/pnas.0900040106, 2009.
- 30 Moffet, R. C., de Foy, B., Molina, L. T., Molina, M. J. and Prather, K. A.: Measurement of ambient aerosols in northern Mexico City by single particle mass spectrometry, *Atmos. Chem. Phys.*, 8(16), 4499–4516, doi:10.5194/acp-8-4499-2008, 2008.
- 35 Murphy, D.: The design of single particle laser mass spectrometers, *Mass Spectrom. Rev.*, (26), 150–165, doi:10.1002/mas, 2007.
- Murray, K. K. and Russell, D. H.: Aerosol matrix-assisted laser desorption ionization mass spectrometry., *J. Am. Soc. Mass Spectrom.*, 5(1), 1–9, doi:10.1016/1044-0305(94)85077-1, 1994.
- Neubauer, K. R., Johnston, M. V. and Wexler, A. S.: Humidity effects on the mass spectra of single aerosol particles, *Atmos. Environ.*, 32(14–15), 2521–2529, 1998.
- 40 Onasch, T. B., Trimborn, A., Fortner, E. C., Jayne, J. T., Kok, G. L., Williams, L. R., Davidovits, P. and Worsnop, D. R.: Soot Particle Aerosol Mass Spectrometer: Development, Validation, and Initial Application, *Aerosol Sci. Technol.*, 46(7), 804–817, doi:10.1080/02786826.2012.663948, 2012.
- 45 Onasch, T. B., Fortner, E. C., Trimborn, A. M., Lambe, A. T., Tiwari, A. J., Marr, L. C., Corbin, J. C., Mensah, A. A., Williams, L. R., Davidovits, P. and Worsnop, D. R.: Investigations of SP-AMS Carbon Ion Distributions as a Function of Refractory Black Carbon Particle Type, *Aerosol Sci. Technol.*, 49(6), 409–422, doi:10.1080/02786826.2015.1039959, 2015.
- Park, K., Kittelson, D. B., Zachariah, M. R. and McMurry, P. H.: Measurement of inherent material density



- of nanoparticle agglomerates, *J. Nanoparticle Res.*, 6, 267–272, 2004.
- Pratt, K., Mayer, J. and Holecek, J.: Development and characterization of an aircraft aerosol time-of-flight mass spectrometer, *Anal. Chem.*, 81(5), 1792–1800, doi:10.1029/2003JD004198.(11), 2009.
- Pratt, K. A. and Prather, K. A.: Mass spectrometry of atmospheric aerosols--recent developments and applications. Part II: On-line mass spectrometry techniques., *Mass Spectrom. Rev.*, 31(1), 17–48, doi:10.1002/mas.20330, 2012.
- Ramanathan, V. and Carmichael, G.: Global and regional climate changes due to black carbon, *Nat. Geosci.*, 1(4), 221–227, doi:10.1038/ngeo156, 2008.
- Reid, J. S. and Hobbs, P. V.: Physical and optical properties of young smoke from individual biomass fires in Brazil, *J. Geophys. Res. Atmos.*, 103(D24), 32013–32030, doi:10.1029/98JD00159, 1998.
- Reid, J. S., Koppmann, R., Eck, T. F. and Eleuterio, D. P.: A review of biomass burning emissions part II: intensive physical properties of biomass burning particles, *Atmos. Chem. Phys.*, 5(3), 799–825, doi:10.5194/acp-5-799-2005, 2005.
- Reinard, M. S. and Johnston, M. V: Ion formation mechanism in laser desorption ionization of individual nanoparticles., *J. Am. Soc. Mass Spectrom.*, 19(3), 389–99, doi:10.1016/j.jasms.2007.11.017, 2008.
- Saliba, G., Subramanian, R., Saleh, R., Ahern, A. T., Lipsky, E., Tasoglou, A., Sullivan, R. C., Bhandari, J., Mazzoleni, C. and Robinson, A. L.: Optical properties of black carbon in cook stove emissions coated with secondary organic aerosols: Measurements and modeling, *Aerosol Sci. Technol.*, n.d.
- Schwarz, J. P., Gao, R. S., Spackman, J. R., Watts, L. A., Thomson, D. S., Fahey, D. W., Ryerson, T. B., Peischl, J., Holloway, J. S., Trainer, M., Frost, G. J., Baynard, T., Lack, D. A., de Gouw, J. A., Warneke, C. and Del Negro, L. A.: Measurement of the mixing state, mass, and optical size of individual black carbon particles in urban and biomass burning emissions, *Geophys. Res. Lett.*, 35(13), L13810, doi:10.1029/2008GL033968, 2008.
- Schwarz, J. P., Spackman, J. R., Gao, R. S., Perring, A. E., Cross, E., Onasch, T. B., Ahern, A., Wrobel, W., Davidovits, P., Olfert, J., Dubey, M. K., Mazzoleni, C. and Fahey, D. W.: The Detection Efficiency of the Single Particle Soot Photometer, *Aerosol Sci. Technol.*, 44(8), 612–628, doi:10.1080/02786826.2010.481298, 2010.
- Shilling, J. E., Chen, Q., King, S. M., Rosenoern, T., Kroll, J. H., Worsnop, D. R., McKinney, K. A. and Martin, S. T.: Particle mass yield in secondary organic aerosol formed by the dark ozonolysis of α -pinene, *Atmos. Chem. Phys.*, 8(7), 2073–2088, doi:10.5194/acp-8-2073-2008, 2008.
- Silva, P. J., Liu, D.-Y., Noble, C. A. and Prather, K. A.: Size and Chemical Characterization of Individual Particles Resulting from Biomass Burning of Local Southern California Species, *Environ. Sci. Technol.*, 33(18), 3068–3076, doi:10.1021/es980544p, 1999.
- Slowik, J., Stainken, K., Davidovits, P., Williams, L. R., Jayne, J. T., Kolb, C. E., Worsnop, D., Rudich, Y., DeCarlo, P. and Jimenez, J.: Particle Morphology and Density Characterization by Combined Mobility and Aerodynamic Diameter Measurements. Part 2: Application to Combustion-Generated Soot Aerosols as a Function of Fuel Equivalence Ratio, *Aerosol Sci. Technol.*, 38(12), 1206–1222, doi:10.1080/02786826.2004.10399462, 2004.
- Slowik, J. G., Cross, E. S., Han, J.-H., Davidovits, P., Onasch, T. B., Jayne, J. T., Williams, L. R., Canagaratna, M. R., Worsnop, D. R., Chakrabarty, R. K., Moosmüller, H., Arnott, W. P., Schwarz, J. P., Gao, R.-S., Fahey, D. W., Kok, G. L. and Petzold, A.: An Inter-Comparison of Instruments Measuring Black Carbon Content of Soot Particles, *Aerosol Sci. Technol.*, 41(3), 295–314, doi:10.1080/02786820701197078, 2007.
- Spencer, M. T. and Prather, K. A.: Using ATOFMS to Determine OC/EC Mass Fractions in Particles, *Aerosol Sci. Technol.*, 40(8), 585–594, doi:10.1080/02786820600729138, 2006.
- Steele, P. T., Srivastava, A., Pitesky, M. E., Ferguson, D. P., Tobias, H. J., Gard, E. E. and Frank, M.: Desorption/ionization fluence thresholds and improved mass spectral consistency measured using a



- flattop laser profile in the bioaerosol mass spectrometry of single *Bacillus* endospores., *Anal. Chem.*, 77(22), 7448–54, doi:10.1021/ac051329b, 2005.
- Stephens, M., Turner, N. and Sandberg, J.: Particle identification by laser-induced incandescence in a solid-state laser cavity., *Appl. Opt.*, 42(19), 3726–3736, doi:10.1364/AO.42.003726, 2003.
- 5 Stockwell, C. E., Veres, P. R., Williams, J. and Yokelson, R. J.: Characterization of biomass burning emissions from cooking fires, peat, crop residue, and other fuels with high-resolution proton-transfer-reaction time-of-flight mass spectrometry, *Atmos. Chem. Phys.*, 15(2), 845–865, doi:10.5194/acp-15-845-2015, 2015.
- Sullivan, R. C. and Prather, K. A.: Recent Advances in Our Understanding of Atmospheric Chemistry and Climate Made Possible by On-Line Aerosol Analysis Instrumentation, *Anal. Chem.*, 77(12), 3861–3886, doi:10.1021/ac050716i, 2005.
- 10 Sullivan, R. C., Guazzotti, S. A., Sodeman, D. A. and Prather, K. A.: Direct observations of the atmospheric processing of Asian mineral dust, *Atmos. Chem. Phys.*, 7(5), 1213–1236, doi:10.5194/acp-7-1213-2007, 2007.
- 15 Sullivan, R. C., Moore, M. J. K., Petters, M. D., Kreidenweis, S. M., Roberts, G. C. and Prather, K. A.: Timescale for hygroscopic conversion of calcite mineral particles through heterogeneous reaction with nitric acid, *Phys. Chem. Chem. Phys.*, 11(36), 7826, doi:10.1039/b904217b, 2009.
- Svane, M., Hagström, M. and Pettersson, J.: Chemical Analysis of Individual Alkali-Containing Aerosol Particles: Design and Performance of a Surface Ionization Particle Beam Mass Spectrometer, *Aerosol Sci. Technol.*, 38(7), 655–663, doi:10.1080/02786820490485944, 2004.
- 20 Thomson, D. S., Schein, M. E. and Murphy, D. M.: Particle Analysis by Laser Mass Spectrometry WB-57F Instrument Overview, *Aerosol Sci. Technol.*, 33(1-2), 153–169, doi:10.1080/027868200410903, 2000.
- Thomson, S., Middlebrook, A. M. and Murphy, D. M.: Thresholds for Laser-Induced Ion Formation from Aerosols in a Vacuum Using Ultraviolet and Vacuum-Ultraviolet Laser Wavelengths, *Aerosol Sci. Technol.*, 26(1993), 544–559, 1997.
- 25 Wenzel, R. J. and Prather, K. A.: Improvements in ion signal reproducibility obtained using a homogeneous laser beam for on-line laser desorption/ionization of single particles., *Rapid Commun. Mass Spectrom.*, 18(13), 1525–33, doi:10.1002/rcm.1509, 2004.
- Willis, M. D., Lee, A. K. Y., Onasch, T. B., Fortner, E. C., Williams, L. R., Lambe, A. T., Worsnop, D. R. and Abbatt, J. P. D.: Collection efficiency of the soot-particle aerosol mass spectrometer (SP-AMS) for internally mixed particulate black carbon, *Atmos. Meas. Tech.*, 7(12), 4507–4516, doi:10.5194/amt-7-4507-2014, 2014.
- 30 Yokelson, R. J., Crouse, J. D., DeCarlo, P. F., Karl, T., Urbanski, S., Atlas, E., Campos, T., Shinozuka, Y., Kapustin, V., Clarke, A. D., Weinheimer, A., Knapp, D. J., Montzka, D. D., Holloway, J., Weibring, P., Flocke, F., Zheng, W., Toohey, D., Wennberg, P. O., Wiedinmyer, C., Mauldin, L., Fried, A., Richter, D., Walega, J., Jimenez, J. L., Adachi, K., Buseck, P. R., Hall, S. R. and Shetter, R.: Emissions from biomass burning in the Yucatan, *Atmos. Chem. Phys.*, 9(15), 5785–5812, doi:10.5194/acp-9-5785-2009, 2009.
- Zandberg, E. Y.: Surface Ionization Detection of Particles, *Tech. Phys.*, 40, 865–884, 1995.
- 40 Zauscher, M. D., Wang, Y., Moore, M. J. K., Gaston, C. J. and Prather, K. A.: Air quality impact and physicochemical aging of biomass burning aerosols during the 2007 San Diego wildfires, *Environ. Sci. Technol.*, 47(14), 7633–7643, doi:10.1021/es4004137, 2013.
- Zelenyuk, A., Yang, J., Choi, E. and Imre, D.: SPLAT II: An Aircraft Compatible, Ultra-Sensitive, High Precision Instrument for In-Situ Characterization of the Size and Composition of Fine and Ultrafine Particles, *Aerosol Sci. Technol.*, 43(5), 411–424, doi:10.1080/02786820802709243, 2009.
- 45 Zhang, J., Huff Hartz, K. E., Pandis, S. N. and Donahue, N. M.: Secondary Organic Aerosol Formation from Limonene Ozonolysis: Homogeneous and Heterogeneous Influences as a Function of NO_x, *J. Phys. Chem. A*, 110(38), 11053–11063, doi:10.1021/jp062836f, 2006.